A PROCEDURE FOR THE IDENTIFICATION OF THE INERTIAL PROPERTIES OF SMALL-SIZE RUAVs

Carlo L. Bottasso*, Domenico Leonello*, Andrea Maffezzoli*, and Fabio Riccardi†

*Dipartimento di Ingegneria Aerospaziale,
Politecnico di Milano, Milano, Italy
e-mail: carlo.bottasso@polimi.it

† Aermatica SpA,
Venegono Superiore (VA), Italy
e-mail: fabio.riccardi@aermatica.com

Abstract

In this paper we consider the problem of estimating the inertial properties of small-size rotorcraft vehicles. The proposed procedure consists in first subjecting the vehicle to a pendular motion; next, time histories of attitude and angular velocity are obtained by using an inertial measurement unit attached to the vehicle; finally, estimates of the inertia tensor components are obtained by using maximum-likelihood constrained optimization in the time domain. The experimental equipment is extremely simple to realize and of low cost.

An important highlight of the proposed approach is that the inertial properties of the vehicle are estimated using specific experimental observations which can be conducted in the laboratory prior to performing flight testing. Hence, flight trials can focus of the sole estimation of the aerodynamic parameters, easing the problem and improving the quality of the estimates.

The procedure is first tested in a simulated environment, by artificially creating virtual time histories so as to verify the observability of all parameters. Then, the procedure is validated by using an object of known inertial characteristics. Finally, the document is concluded with the application of the proposed methodology to a small rotorcraft vehicle.

1 INTRODUCTION

Mathematical models of aerial vehicles are crucial for enabling the myriad simulation needs that support the vehicle design and operation, including the synthesis of model-based control laws. To ensure the best possible fidelity of each given model to the plant, suitable methods are formulated for extracting best (in a statistical sense) estimates of the model parameters from experimental observations. Parameter estimation problems are notoriously difficult to solve, since the problem is often ill posed, presents multiple local solutions, is affected by scarce observability of some parameters, and is corrupted by measurement and possibly process noise.

In most cases, including for example the rotary wing class of vehicles, the highest level of uncertainty is in the aerodynamic components of the model, which describe complex non-linear physical processes which profoundly determine the vehicle response characteristics. Unfortunately, the inertial parameters of the vehicle also have a strong effect on its dynamics, and must be known precisely. Being difficult to measure with accuracy, unless one can weight all vehicle components and has precise knowledge of their location [2, 13], the vehicle inertial quantities are often estimated *together* with the aerodynamic parameters from flight test data, which complicates the estimation problem by increasing the number of unknowns.

To address these issues, in this paper we present a method for estimating the inertial properties of small rotorcraft vehicles using specific experimental observations which may be conducted in the laboratory *prior* to performing flight testing. This way, the parameter estimation performed from flight test data can be limited to the sole estimation of the aerodynamic parameters, easing the problem and in turn improving the quality of the estimates.

Several methods for the estimation of the inertial characteristics of rigid bodies have been presented in the literature.

In some of the proposed methods the object is constrained to rotate about one axis and, by measuring the frequency of oscillation about the pivot axis, the value of the moment of inertia around that axis is determined by solving a least-squares identification problem [3, 12]. By changing the orientation of the rotation axis with respect to the object, one can mea-

sure the various components of the inertia tensor, although this requires a special hardware and multiple experiments.

Other approaches use special measurement robots which subject the object to desired motions [7, 11]. Although these approaches can identify all unknown inertia parameters in a rigid body, the measurement robots are typically rather complex and expensive machines.

Yet other methods have been proposed which use frequency response functions and/or modal analysis to identify the inertia parameters, often together with the stiffness and damping characteristics of the mount elements [1, 5, 6]. The simplest and most effective arrangements are based on suspending the object by means of one or more cables and making it swing freely [4, 8, 10]. The recorded time histories of angular velocity, acceleration and attitude of the object are then numerically processed so as to estimate the elements of the inertia tensor.

In this paper we present a method based on pendular motions. The object is suspended by using a spherical mount. Next, the response during a free pendular motion is measured by a high-accuracy inertial measurement unit (IMU) fixed to the object. Finally, estimates of the inertial parameters are obtained together with estimates of the aerodynamic coefficients experienced by the object in its pendular motions and of the friction coefficients at the mounting pivot. Since the estimation of these unknowns is a non-linear parameter estimation problem in the presence of measurement noise, we use the time-domain Output Error Method (OEM) [9], which amounts to a constrained optimization problem of a maximum-likelihood cost function. The approach deals rigorously with the presence of measurement noise, can use simultaneously time histories from multiple experiments for improving the quality of the estimates, and allows one to enforce constraints on the unknown parameters, for example for ensuring physically meaningful results at convergence. Furthermore, the experimental hardware is extremely simple and of low cost, the only significant item being the IMU.

At first, we describe the experimental set-up and we formulate the proposed approach. Next, we present simulated experiments performed in order to test the procedure and verify the observability of the unknown parameters. Then, we describe tests conducted for the validation of the procedure using an object of known inertial characteristics. Finally, we describe an application of the presented method to a small-size rotorcraft unmanned aerial vehicle (UAV).

2 INERTIA ESTIMATION PROCEDURE

2.1 Experimental Set-Up

The estimation of the components of the inertia tensor of a rigid body can be performed by subjecting the object to a pendular motion. Figure 1 shows a small rotorcraft UAV: a supporting structure is made of a steel plate with a flared hole in the middle and of four steel rods; the supporting structure is suspended to a emisphere, which is in turn connected to a supporting frame. If the emisphere is properly lubricated, the connection works as a spherical joint with small friction. In the present implementation, this arrangement allows for roll and pitch oscillations of up to 35 deg of amplitude, and for 360 deg yawing rotations.

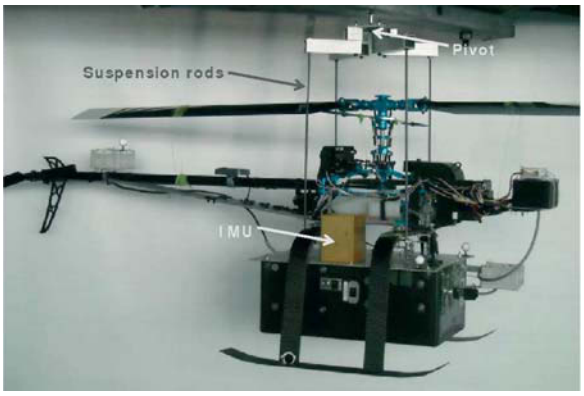

Figure 1: Small rotorcraft UAV with steel rods and IMU, suspended at a pivot point.

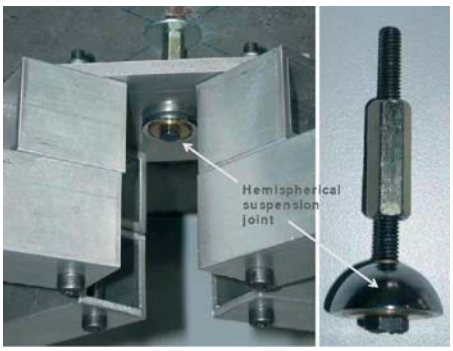

Figure 2: Detail of the pivot.

The compound system, composed by the helicopter and the supporting structure, has a known mass and center of gravity position and can be modeled as a rigid pendulum.

2.2 Equations of Motion

By suddenly cutting a suspension string holding the vehicle at rest at a given initial attitude, the system starts oscillating and its motion can be described by Euler second law:

$$\boldsymbol{J}_O\,\dot{\boldsymbol{\omega}} + \boldsymbol{\omega} \times \boldsymbol{J}_O\,\boldsymbol{\omega} = \boldsymbol{m}_O, \tag{1}$$

where $\boldsymbol{\omega}$ is the body angular velocity and $\boldsymbol{m}_O$ is the moment of all external forces about the pivot point O. $\boldsymbol{J}_O$ is the inertia tensor of the vehicle and of the support structure about the same pivot point

$$\boldsymbol{J}_O = \boldsymbol{J}_{O_{\text{vehicle}}} + \boldsymbol{J}_{O_{\text{struct}}}, \tag{2}$$

where, by the parallel axis theorem, we have

$$\boldsymbol{J}_{O_{\text{vehicle}}} = \boldsymbol{J}_G + m\left((\boldsymbol{r}_{OG}^T\,\boldsymbol{r}_{OG})\boldsymbol{I} - (\boldsymbol{r}_{OG}\,\boldsymbol{r}_{OG}^T)\right), \tag{3}$$

$\boldsymbol{J}_G$ being the inertia tensor about the vehicle center of gravity G and $\boldsymbol{r}_{OG}$ the distance vector from point O to point G.

The experimental arrangement of Fig. 2 can be modeled as a uniform body hinged at an arbitrary point, as sketched in Fig. 3. The inertial Earth-fixed reference frame $\mathcal{E}$ of unit vectors $(\boldsymbol{e}_1, \boldsymbol{e}_2, \boldsymbol{e}_3)$ is centered at the pivot point O, whereas the body-attached reference frame $\mathcal{B}$ of unit vectors $(\boldsymbol{b}_1, \boldsymbol{b}_2, \boldsymbol{b}_3)$ is centered at G.

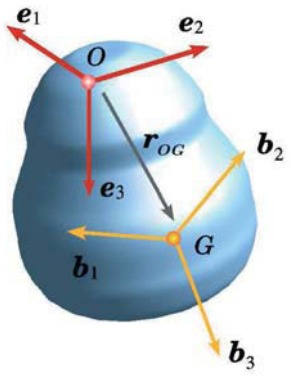

Figure 3: Sketch of the body model with reference frames.

The equations of motion of the rigid body write:

$$\boldsymbol{J}_O^{\mathcal{B}}\dot{\boldsymbol{\omega}}^{\mathcal{B}} + \boldsymbol{\omega}^{\mathcal{B}} \times \boldsymbol{J}_O^{\mathcal{B}}\,\boldsymbol{\omega}^{\mathcal{B}} = \boldsymbol{m}_O^{\mathcal{B}}, \tag{4a}$$

$$\boldsymbol{\omega}^{\mathcal{B}} = \boldsymbol{S}(\boldsymbol{q})\dot{\boldsymbol{q}}, \tag{4b}$$

where the notation $(\cdot)^{\mathcal{B}}$ indicates components of a vector or tensor in frame $\mathcal{B}$, $\boldsymbol{q}$ indicates a set of rotation parameters while $\boldsymbol{S}$ is the parameterization dependent matrix which enables to express the body attached components of the angular velocity in terms of the time rates of change of the rotation parameters; furthermore, the components of the inertia tensor are noted

$$\boldsymbol{J}_O^{\mathcal{B}} = \begin{bmatrix} I_{xx} & I_{xy} & I_{xz} \\ I_{xy} & I_{yy} & I_{yz} \\ I_{xz} & I_{yz} & I_{zz} \end{bmatrix}. \tag{5}$$

The moment of the external forces $\boldsymbol{m}_O$ includes weight, aerodynamic forces and friction at the pivot point, and writes

$$\boldsymbol{m}_O = \boldsymbol{r}_{OG} \times \boldsymbol{w} + \boldsymbol{m}_{O_{\text{frict}}} + \boldsymbol{m}_{O_{\text{aero}}}, \tag{6}$$

where $\boldsymbol{w} = mg\boldsymbol{e}_3$ is the weight vector. The sliding friction moment at the pivot is modeled as

$$\boldsymbol{m}_{O_{\text{frict}}} = -\operatorname{diag}(\mu_{k_1}, \mu_{k_1}, \mu_{k_2})\frac{\boldsymbol{\omega}}{\|\boldsymbol{\omega}\|}, \tag{7}$$

with two different friction coefficients μ_{k_1} and μ_{k_2}, the former for rotations about the $\boldsymbol{b}_1$ and $\boldsymbol{b}_2$ body axes and the latter for rotations about $\boldsymbol{b}_3$, which reflect the physical arrangement of the spherical joint used for the pivot suspension (see Fig. 2).

The aerodynamic moment $\boldsymbol{m}_{O_{\text{aero}}}$ at the pivot point is due to the aerodynamic force (drag) and associated moment about the aerodynamic center C, and can be written as

$$\boldsymbol{m}_{O_{\text{aero}}} = \frac{1}{2}\rho V^2 S(C_m l - C_d\|\boldsymbol{r}_{OC}\|)\frac{\boldsymbol{r}_{OC}}{\|\boldsymbol{r}_{OC}\|} \times \frac{\boldsymbol{v}_C}{V}, \tag{8}$$

where ρ is the air density, $\boldsymbol{v}_C$ is the velocity vector at point C and $V = \|\boldsymbol{v}_C\|$ its speed, S a reference surface, l a reference length, C_m and C_d the body moment and drag coefficients, respectively. Since the two aerodynamic coefficients and the location of the aerodynamic center can not be identified simultaneously from the pendular experiments, a single unknown aerodynamic parameter is defined as

$$p_{\text{aero}} = S(lC_m - C_d\|\boldsymbol{r}_{OC}\|); \tag{9}$$

consequently, assuming that the aerodynamic center is close to the center of gravity, the speed V of C in Eq. (8) is approximated with the speed of the center of gravity G, whose location is known.

The set of non-linear state-space Eqs. (4) for the parametric model $\mathcal{M}(\boldsymbol{p})$ of the experimental set-up can be written in the following compact form:

$$\boldsymbol{f}(\dot{\boldsymbol{x}}, \boldsymbol{x}, \boldsymbol{p}) = 0, \tag{10}$$

where the state vector is $\boldsymbol{x} \doteq (\boldsymbol{\omega}^{\mathcal{B}^T}, \boldsymbol{q}^T)^T$, and the vector of unknown model parameters is $\boldsymbol{p} \doteq (I_{xx}, I_{xy}, I_{xz}, I_{yy}, I_{yz}, I_{zz}, p_{\text{aero}}, \mu_{k_1}, \mu_{k_2})^T$.

2.3 Measures

A high-accuracy IMU is used for measuring the response of the object during its pendular motion (see

Figure 4: Crossbow Fiber Optic Vertical GYRO.

Update rate	1−100 Hz
Attitude range (Roll, Pitch)	± 180 deg, ± 90 deg
Resolution	< 0.1 deg
Heading range	± 180 deg
Resolution	0.1 deg
Angular velocity range	± 200 deg/s
Resolution	< 0.05 deg/s
Acceleration range	± 10 g
Resolution	< 1.25 mg

Table 1: Crossbow Fiber Optic Vertical GYRO specifications.

Fig. 1). The system used in this work is depicted in Fig. 4 and uses a tri-axial gyro, a tri-axial accelerometer and a tri-axial magnetometer; Table 1 shows its technical specifications.

The estimates of the angular velocity $\boldsymbol{\omega}_{\mathrm{IMU}}$ and angular position $\boldsymbol{q}_{\mathrm{IMU}}$ provided by the IMU are affected by noise $\boldsymbol{n}_{\boldsymbol{\omega}}$ and $\boldsymbol{n}_{\boldsymbol{q}}$, respectively, and are available at N discrete sampling time instants t_k. Hence, a set of measurement equations can be written as

$$\boldsymbol{z}(t_k) = \boldsymbol{y}(t_k) + \boldsymbol{\mu}(t_k), \tag{11}$$

where $\boldsymbol{z} \doteq (\boldsymbol{\omega}_{\mathrm{IMU}}^T, \boldsymbol{q}_{\mathrm{IMU}}^T)^T$ is the measurement vector, $\boldsymbol{y} \doteq (\boldsymbol{\omega}^{\mathcal{B}^T}, \boldsymbol{q}^T)^T = \boldsymbol{x}$ is the output vector, and $\boldsymbol{\mu} \doteq (\boldsymbol{n}_{\boldsymbol{\omega}}^T, \boldsymbol{n}_{\boldsymbol{q}}^T)^T$ is the measurement noise vector whose covariance is $\boldsymbol{R}_k = E[\boldsymbol{\mu}_k \boldsymbol{\mu}_k^T]$, $E[\cdot]$ being the expected value operator.

2.4 Parameter Estimation

The OEM method [9] for the estimation of the unknown model parameters in model $\mathcal{M}(\boldsymbol{p})$ can be written as

$$\min_{\boldsymbol{x},\boldsymbol{y},\boldsymbol{p}} \quad J(\boldsymbol{z}-\boldsymbol{y}), \tag{12a}$$

$$\text{s.t.: } \boldsymbol{f}(\dot{\boldsymbol{x}}, \boldsymbol{x}, \boldsymbol{p}) = 0, \tag{12b}$$

$$\boldsymbol{y} = \boldsymbol{h}(\boldsymbol{x}), \tag{12c}$$

$$\boldsymbol{g}(\boldsymbol{p}) \leq 0. \tag{12d}$$

The presence of the measurement noise makes the problem of a stochastic nature. Hence, the optimization cost function J is typically a statistical measure of the difference between measures $\boldsymbol{z}$ and model outputs $\boldsymbol{y}$. A Maximum Likelihood estimator is obtained by choosing

$$J = \det(\boldsymbol{R}), \tag{13}$$

where $\boldsymbol{R} = 1/N \sum_{k=1}^{N} \big(\boldsymbol{z}(t_k) - \boldsymbol{y}(t_k)\big)\big(\boldsymbol{z}(t_k) - \boldsymbol{y}(t_k)\big)^T$. Alternatively, a weighted Least Squares estimator is obtained if

$$J = \frac{1}{2} \sum_{k=1}^{N} \big(\boldsymbol{z}(t_k) - \boldsymbol{y}(t_k)\big) \boldsymbol{W} \big(\boldsymbol{z}(t_k) - \boldsymbol{y}(t_k)\big)^T, \tag{14}$$

where $\boldsymbol{W}$ is a weight matrix. This method can be seen as a particular case of the Maximum Likelihood method for known measurement noise covariance matrix, $\boldsymbol{W} = \boldsymbol{R}^{-1}$ [9]. Inequality (12d) enforces possible constraints on the model parameters. Such constraints ensure that the estimated parameters lie within acceptable bounds and do not take at convergence values which are non-physical.

The Filter Error Method [9] considers also the possible presence of a process noise term in Eq. (12b); this however was not deemed necessary in the present application, since the experiments are conducted in calm air in the laboratory.

3 APPLICATIONS AND RESULTS

3.1 Simulated Identification

To test the identification procedure we carried out a number of *simulated* experiments. This phase is essential for understanding whether the unknown parameters are observable and to what degree, to evaluate the effects of the aerodynamic and joint friction coefficients, to study the effect of measurement noise and therefore to determine the required accuracy of the on-board IMU, and to determine the best practices and procedures for the conduction of the experimental observations.

To this end, system (4) was integrated forward in time from assigned initial conditions and for given realistic values of the parameters of the model and of the experimental equipment, including measurement errors. Of the many tests conducted, we report here only a brief synthesis to illustrate the main conclusions.

Firstly, the aerodynamic contribution to the moment acting on the body is almost negligible if compared to the friction contribution, which is reasonable considering the low speed experienced by the vehicle during its pendular motions. Furthermore, it was observed that the unknown aerodynamic parameter can

be eliminated without noticeable effects on the quality of the estimates of the inertia terms, with a reduction by one of the number of the problem unknowns. Typically this is automatically compensated by a slight overestimate in the value of the converged friction coefficients. Figure 5 reports the time histories of the measures (solid lines) and those produced by the identified model at convergence (dashed lines), which show an excellent matching. Figure 6 shows the convergence history of the inertial parameters, with whiskers indicating the associated standard deviation and a horizontal line indicating the exact solution. Finally, Fig. 7 shows the convergence history of the friction coefficients: it is evident how the friction coefficient μ_{k_1} is slightly overestimated to approximately include the damping contribution of the aerodynamic drag.

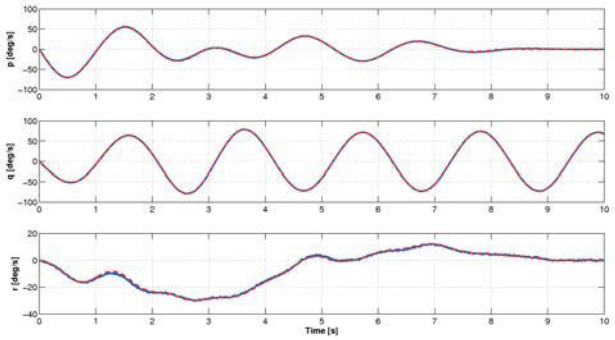

Figure 5: Time histories of the angular velocity body-attached components for a simulated identification experiment. Solid line: IMU-measured response. Dashed line: computed response for converged estimated model.

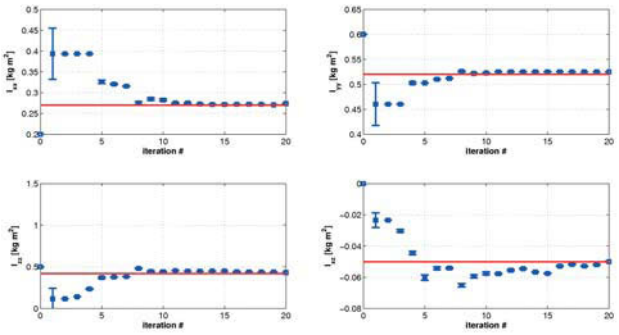

Figure 6: Progress of inertial parameters with standard deviations. Horizontal line: exact values.

Secondly, we observe that the estimation of the inertial parameters is unsatisfactory if the distance from the pivot point to the center of gravity is too large. In fact, referring to Eq. (3), if the contribution of the inertia tensor about the center of gravity, $\boldsymbol{J}_G$, becomes too small with respect to the transport contribution, the

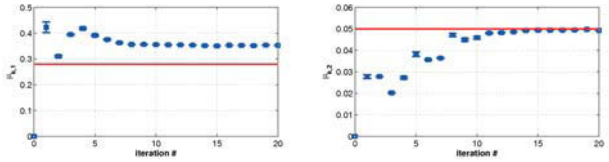

Figure 7: Progress of friction parameters with standard deviations. Horizontal line: exact values.

estimates tend to become inaccurate; with the small-size UAV object of the present study, an acceptable limit for this distance is of about 1 m. Figure 8 shows the response of the identified model performed with a distance from the pivot point to the body center of gravity equal to 2 m, which clearly shows a poor matching indicative of a very imprecise identification.

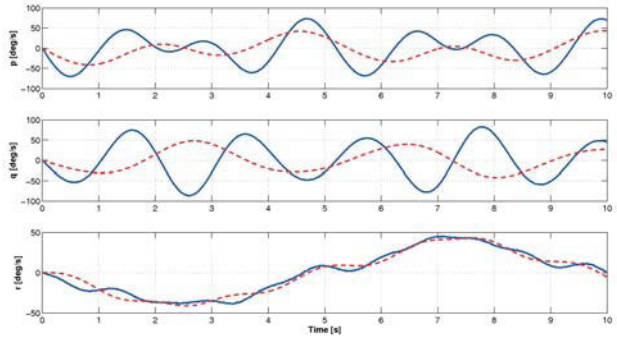

Figure 8: Simulated identification with large distance pivot-center of gravity. Solid line: IMU-measured response. Dashed line: computed response for converged parameter estimation.

Finally, we notice that it is important to choose a suitable amplitude for the initial conditions in order to properly excite the response of the system and guarantee a satisfactory level of observability for all parameters. Tests revealed that, in the present case, estimates begin to be inaccurate with starting values for the roll ϕ and pitch θ angles below $10 \div 15$ deg.

3.2 Procedure Validation

Before attempting the estimation of the inertial parameters of a small-size RUAV, the proposed procedure was validated with the help of a complex object with known inertial properties, having weight and dimensions similar to those of the target RUAV. To this end, we used a steel plate with several holes and added weights, as shown in Fig. 9. The inertial properties were obtained by a detailed CAD model of the object, and by weighting and precisely measuring all components, including the IMU.

Figure 10 and 11 show that the estimated time histories for the converged estimated model fit the measures with reasonable accuracy, which is indicative of

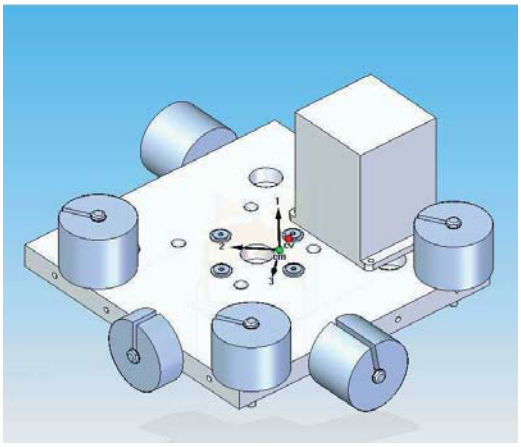

(a) Balanced plate.

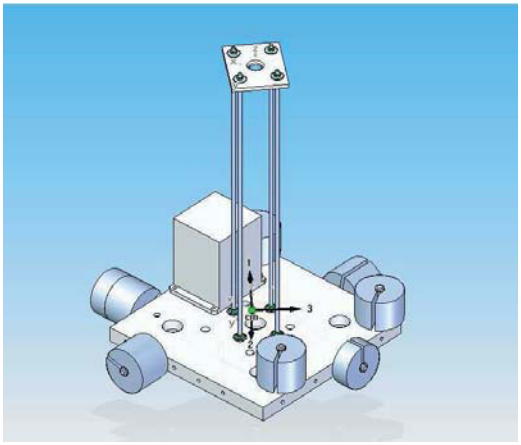

(b) Overall system.

Figure 9: CAD model of the object of known inertial properties used for the validation of the procedure.

a successful identification.

Figure 12 illustrates an example of the convergence history of the moments of inertia of the validation object. The identified values for these parameters lay within a $\pm 5\%$ band from the expected CAD-derived values.

Figure 13 shows the convergence history of the products of inertia of the plate. We observe that the terms I_{xz} and I_{yz} are identified with lower accuracy than in the previous case, due to the fact that these parameters are two orders of magnitude lower than the diagonal moments of inertia. Notice however that the initial guesses were set to zero, and that the converged values are of the correct order of magnitude.

Figure 14 illustrates the convergence history of the friction coefficients of the joint. As their actual value is unknown, we can only appreciate that they show a rapid convergence to reasonable values.

These results seem to support the conclusion that an accurate identification of the inertial properties of an object with weight and dimensions similar to those of the plate used for validation, is possible with the procedure and equipment described above.

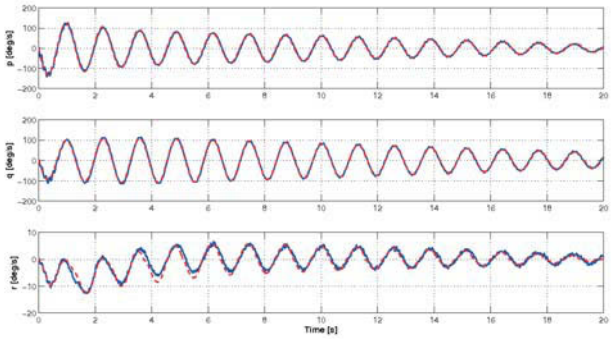

Figure 10: Plate angular velocity body-attached components. Solid line: IMU-measured response. Dashed line: computed response for converged parameter estimation.

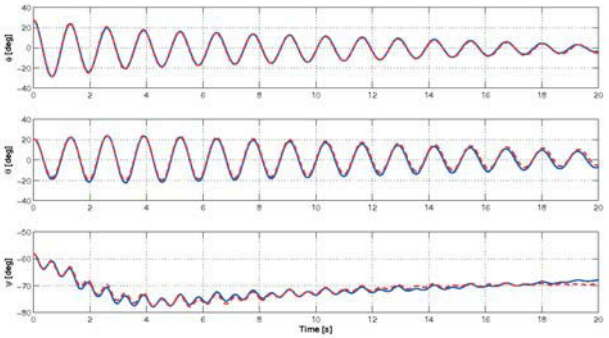

Figure 11: Plate Euler angles. Solid line: IMU-measured response. Dashed line: computed response for converged parameter estimation.

3.3 Application to a Small-Size RUAV

The RUAV is tested with an empty fuel tank, to avoid sloshing during the pendular motions. Figure 15 shows the configuration during the experiments, the supporting structure and the connection to a large portal used for suspending the whole apparatus. The experiment was conducted without the rotor blades, although the figure shows the opposite, since they will occupy different azimuthal configurations during flight; their (modest) contribution to the inertia of the vehicle was estimated by simply weighting them and measuring the location of their center of gravity along the span.

We performed several experiments starting from different initial conditions. For the identification, we considered all time responses that showed an adequate excitation of the three angular velocities and the three Euler angles, according to the indications coming from the simulated identification tests. The starting angular velocity was set to zero for each experiment, since the oscillations always started from an

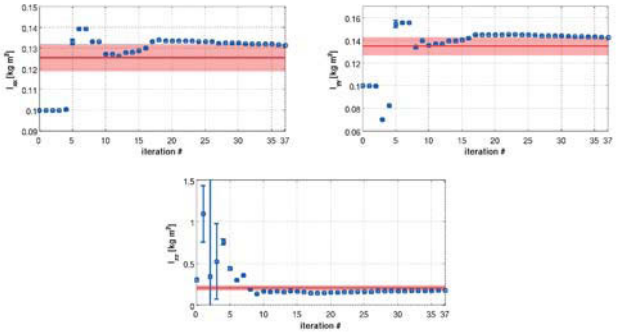

Figure 12: Progress of moments of inertia with standard deviations. Horizontal line: “exact” CAD-derived values. Light band: error bounds.

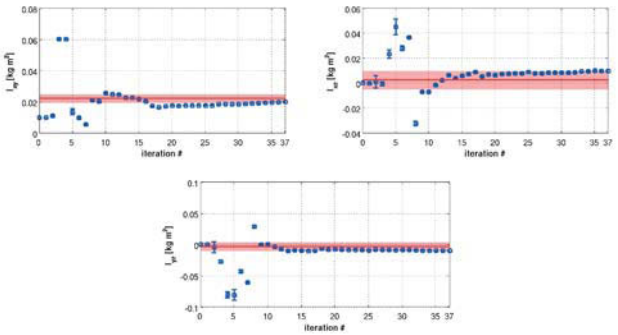

Figure 13: Progress of products of inertia with standard deviations. Horizontal line: “exact” CAD-derived values. Light band: error bounds.

initial condition at rest by cutting a restraining string.

The time histories for the converged estimated model show a good agreement with the time histories measured from the pendular tests for all selected experiments, as shown in Fig. 16 and 17. It appears that the measured time histories present a high-frequency component of the response, probably due to the elasticity of the supporting structure. Clearly, such component of the solution is absent from the identified model, since it is based on the rigid body assumption.

The numerical values of the identified parameters are presented in Table 2. Each identified value is the mean value obtained by several identification runs starting from different initial guesses for the parameters, and it is shown together with its standard deviation. Overall, the results indicate that the moments of inertia I_{xx}, I_{yy} and I_{zz} and the friction coefficients μ_{k_1} and μ_{k_2} show a good precision, with standard deviations within $5-15\%$ of the respective mean values. Similarly to the validation problem, it appears that the product of inertia I_{xz} has a lower degree of precision.

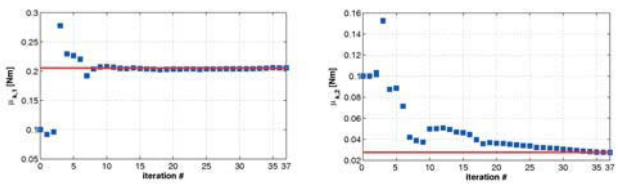

Figure 14: Progress of friction coefficients with standard deviations. Horizontal line: converged values.

(a) Supporting structure.

(b) Helicopter hung to portal.

Figure 15: RUAV configuration for pendulum experiments.

Figure 18 illustrates an example of the convergence history of the moments of inertia of the helicopter, with the standard deviations at each iteration shown by using whiskers. The estimate of I_{yy} is characterized by a higher precision than the other inertia parameters, while the worst precision is associated to the product of inertia I_{xz}.

Figure 19 illustrates an example of the convergence history of the friction coefficients at the suspension joint. It appears that both estimates are characterized by a good accuracy.

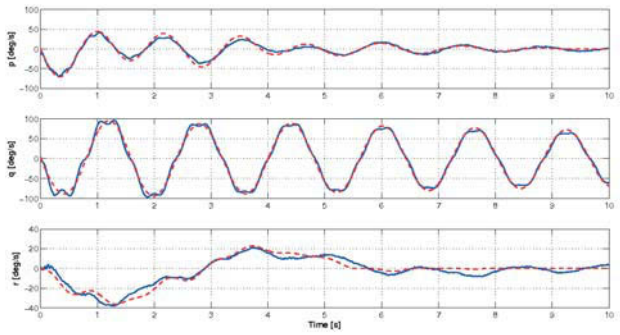

Figure 16: RUAV estimation problem, angular velocity body-attached components. Solid line: IMU-measured response. Dashed line: computed response for converged parameter estimation.

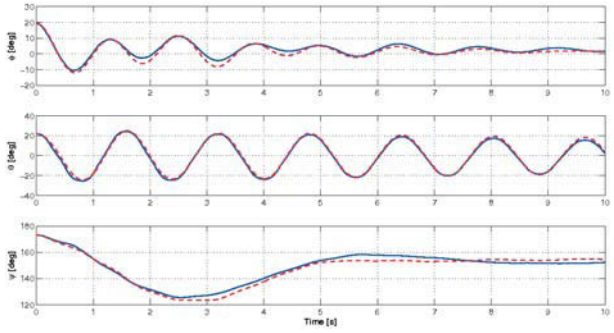

Figure 17: RUAV estimation problem, Euler angles. Solid line: IMU-measured response. Dashed line: computed response for converged parameter estimation.

4 CONCLUSIONS

In this paper we have presented a method for estimating the inertia tensor of a small-size rotorcraft vehicle. It was shown that accurate identification of the inertial parameters of such a vehicle can be achieved by using specific experimental observations which may be conducted in the laboratory, prior to performing the flight tests necessary for the estimation of its aerodynamic characteristics. The procedure consists in subjecting the vehicle to a pendular motion, and recording its response. From the measured response, estimates of the unknown model parameters are computed using a maximum likelihood time-domain optimization, which accounts for the stochastic nature of the problem due to the presence of measurement noise.

Id. Parameter	Mean Value	Standard Dev.
I_{xx} [kg m^2]	0.171	0.019
I_{yy} [kg m^2]	0.898	0.038
I_{zz} [kg m^2]	0.932	0.066
I_{xz} [kg m^2]	-0.055	0.063
μ_{k_1} [Nm]	0.248	0.026
μ_{k_2} [Nm]	0.115	0.018

Table 2: Estimated inertial properties of the RUAV and joint friction coefficients.

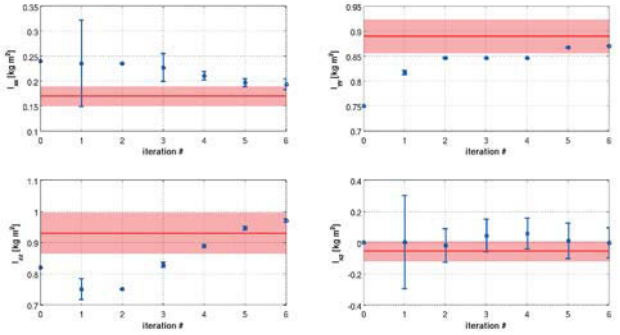

Figure 18: Progress of inertial parameters with standard deviations. Horizontal line: final identified value. Light band: standard deviation of final identified value.

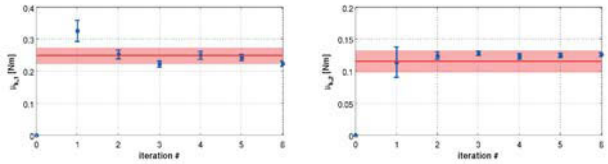

Figure 19: Progress of parameters with standard deviations. Horizontal line: final identified value. Light band: standard deviation of final identified value.

The results have shown a very satisfactory agreement between measured and computed responses, which indicates a successful identification of the unknown inertial parameters and confirms the suitability of the approach for the present scopes.

We have argued that performing simulated identification tests from virtual experiments and validating the procedure with an object of known characteristics, provides helpful information on the design of the experimental set-up, on the tuning of the procedure and on the identification of best practices for conducting the experiments.

Specific conclusions which have emerged from the present work can be summarized as follows:

- Aerodynamic forces during pendular motion are negligible if compared to the friction contribution: the elimination of the aerodynamic terms from the model simplifies the identification process and leads to good agreement between measured and simulated responses, with a small overestimate of the friction coefficients;

- The distance from the pivot point to the vehicle center of gravity must be small enough to mini-

mize the transport contribution to the inertia tensor;

- Suitable amplitudes for the initial attitudes must be chosen in order to properly excite the system response and guarantee a satisfactory level of observability for all parameters;

- The validation of the method with an object with known inertial properties indicates that the diagonal moments of inertia can be identified within a $\pm 5\%$ of accuracy, which was judged sufficient for the present application;

- The application of the proposed method to a small-size rotorcraft UAV with unknown inertial properties lead to estimates of the moments of inertia and friction parameters with standard deviations within $5 \div 15\%$ of their respective mean values.

References

[1] R.A.B. Almeida, A.P.V. Urgueira, N.M.M. Maia. Identification of rigid body properties from vibration measurements. *Journal of Sound and Vibration*, **299**, 884–899, 2007.

[2] E.V. Buyanov. Device for measuring the inertia tensor of a rigid body. *Journal of Measurement Techniques*, **34**(6), 585–589, 1991.

[3] M. Da Lio, A. Doria, R. Lot. A spatial mechanism for the measurement of the inertia tensor: theory and experimental results. *Journal of Dynamic Systems, Measurement, and Control*, **121**, 111–116, 1999.

[4] C. Doniselli, M. Gobbi, G. Mastinu. Measuring the inertia tensor of vehicles. *Vehicle System Dynamics Supplement*, **37**, 301–313, 2002.

[5] A. Fregolent, A. Sestieri. Identification of rigid body inertia properties from experimental frequency response. *Journal of Mechanical Systems and Signal Processing*, **10**, 697–709, 1996.

[6] A. Gentile, L. Mangialardi, G. Mantriota, A. Trentadue. Measurement of the inertia tensor: an experimental proposal. *Journal of Measurement*, **16**, 241–254, 1995.

[7] H. Hahn, M. Niebergall. Development of a measurement robot for identifying all inertia parameters of a rigid body in a single experiment. *IEEE Transactions on Control Systems Technology*, **9**, 416–423, 2001.

[8] M.R. Jardin, E.R. Mueller. Optimized measurements of UAV mass moment of inertia with a bifilar pendulum. AIAA Guidance, Navigation and Control Conference and Exhibit, Hilton Head, SC, USA, 2007.

[9] R.V. Jategaonkar. *Flight Vehicle System Identification: A Time Domain Methodology*. Progess in Astronautics and Aeronautics, Vol. 216, AIAA, Reston, VA, 2006.

[10] M.D. McEwen. *Dynamic System Identification and Modeling of a Rotary Wing UAV for Stability and Control Analysis*. Naval Postgraduate School, Monterey, CA, USA, 1998.

[11] V.G. Melnikov. A new method for inertia tensor and center of gravity identification. *Nonlinear Analysis*, **63**, 1377–1382, 2005.

[12] M. Niebergall, H. Hahn. Identification of the ten inertia parameters of a rigid body. *Journal of Nonlinear Dynamics*, **13**, 362–371, 1997.

[13] R.S. Sharp. The measurement of mass and inertial properties of vehicles and components. *Autotech*, 1997.